Resonant sensors for multi-axis force and torque estimation in collaborative robotics

Davinson Castano-Cano, Mathieu Grossard, Arnaud Hubert

Resonant Sensors for Multi-axis Force and Torque Estimation in Collaborative Robotics

Davinson Castano-Cano, Mathieu Grossard and Arnaud Hubert

Corresponding author: e-mail: mathieu.grossard@cea.fr, tel: +33(0)169080787, fax: +33(0)169080701
EAFIT University, Colombia
Université Paris-Saclay, CEA, List, F-91120, Palaiseau, France
Université de Technologie de Compiegne, Roberval (Mechanics, energy and electricity), centre de recherche de Royallieu, CS 60319, 60203 Compiegne cedex, France.

Abstract

This paper presents a complete design methodology for a multi-axis resonant force sensor. The proposed device has been designed to be usable in a context of physical interaction between robots and humans. The proposed solution allows the three force components and the three torque components to be measured simultaneously and can be inserted into an interface handle or a robot end-effector. The information on wrench can then be used to detect and control interactions for cooperative tasks between humans and robots. In the context of sensors for robotic co-manipulation, it is imperative to guarantee not only a certain level of performance (accuracy, dynamics, size) but also to guarantee certain non-functional specifications associated with safety, measurement redundancy or functional integration of the sensor into its environment. The consideration of all these design specifications, both functional and non-functional, led to the principles and technologies used to develop this sensor. Multi-axis resonant sensors have excellent performance and safety characteristics, two key elements for collaborative robotics, but the literature review did not reveal any significant previous work in this area. Thus, this paper proposes an original sensor based on a breakthrough technology in the crucial field of multi-axis force sensors. The performances obtained on our prototype are already close to the performances of the best existing 6-axis industrial sensors, which suggests very good prospects for this new technology. In addition, and compared to alternative technologies, resonance technology offers new possibilities in terms of sensor fault detection, thus improving the intrinsic safety of these devices.

Key words: Multi-axis force sensors, wrench estimation, resonant transducers, collaborative robotics.

1. Introduction

The use of force-controlled robots is increasing and is expected to become widespread in the near future. Theses robots are currently used in a wider range of applications, well beyond the context of traditional industrial robotics. Examples of such applications are assistance to humans for service tasks, assistance to operators for carrying loads, performing advanced manipulation tasks, etc. There is an ever-increasing need to develop robots capable of physical interaction with the environment or even humans, [38].

In the physical Human Robot Interaction (pHRI) context, force/impedance control schemes seem to be a convenient and crucial way for implementing human and robot co-manipulation strategies. For example, when considering the pHRI Hands-On context, performing direct force/torque (F/T) control offers the possibility of controlling the contact F/T to a desired value thanks to the closure of a feedback loop. Such interaction tasks require the fulfilment of a value of the contact force at the interface between the robot and the human hand. Among the different solutions to deal with force sensitivity for robot arms, the use of external force/torque sensors remains the most straightforward way to give the robot the capability of controlling physical interaction with its environment. Providing such handle interface with an external 6-axis F/T sensory apparatus can ensure the capability of sensing and controlling exchanged forces for cooperating tasks between humans and robots [51]. Possible targeted uses in this particular collaborative robotic field considers human/robot interaction that can be performed for short periods of time, for example, when the operator teaches the robots the trajectory to respect, and also for longer periods of time when the robot assists continuously humans.

To achieve specifically this milestone, safety is a major concern that need to be considered at hardware level for designing inherently safe 6-axis F/T sensors. In this perspective, principles and technologies exploited for the transducer, as well as its functional integration into the sensor body device, remain key factors to define performance and modality of the design with respect to safety. As starting point of this paper, it is important to note that force is an intensive property and thus, it cannot be measured directly, but through a test-body: a mechanical structure is required to convert applied forces to measurable physical quantities. Traditional force sensors get the information on applied force through measurements of deformation or displacement of test-bodies. Resonant sensors get this information through resonant frequencies of test-bodies. Different physical principles can be used to estimate external forces, such as optical-based force sensors, [16, 49, 60], sensing capacitance array, [10, 20, 53], MEMS barometers [30] or MEMS-based fabri-

cation process of sensor chips [36, 47], strain gauges,[35, 54], which is the most used technology. Different structures are used as test-bodies for the strain gauges technology, some examples are: Hollow Hexaform structures, [1] for torque sensors, Steering wheel or Maltese cross shape for force sensors, [15], modularized assembly of 1-D force sensors, [59], structures based on parallel *Stewart* kinematics, [63]. Some of these sensor test-bodies are represented in Figure 1.

These sensors can be fairly stiff and robust. However, strain-gauge-based sensor signals present drift and noise issues and their manufacturing processes are expensive (because severe and precise requirements on the machining, assembly and calibration of the integrated structure are needed), [29]. These inconveniences can be overcome using the resonant principle. This promising alternative presents noise immunity, high sensitivity and good stability [5]. Indeed, a great advantage lies in their easy way to measure frequency shift, and their reduced manufacturing cost, [39]. Since induced static stresses due to external forces slightly change the stiffness properties of the force-vibrating structure, a slight frequency shift occurs. Resonant sensors are active structures embedding actuating and sensing elements to track these resonance frequencies.

This paper is organized as follows. Section 2 is based on a force sensor survey focusing on robotic applications. It provides different classifications depending on their characteristics and technologies. We extend the description of the general anatomy of a force sensor, before presenting the founding principle of resonant sensors. In Section 3, guidelines for designing a modular multi-axes sensor are introduced. It provides the design of a modular sensitive element that exhibits suitable properties regarding the application requirements. Section 4 focuses on the design rationale of the whole sensor structure, including several sensitive elements as modules. Section 5 contains the test performed on the multi-axis force sensor prototype. An analysis of the obtained performances of the sensor is presented with respect to the targeted application. Finally, conclusions and future lines of work are proposed in Section 6.

2. State-of-the-Art Force Sensors Technologies

2.1. General Overview on Force Sensors

The study of force sensors can be split into two main categories depending on their conversion type, [8] (see Figure 1): composite and direct conversion.

- Composite conversion force sensors estimate the applied force by measuring the strain or displacement of a specific part of the test-body.
- Direct conversion force sensors estimate the applied force by measuring other physical quantities affected by the test-body stress response. Resonant sensors belong to this group. In such a case, frequencies are the measured physical quantities.

These two types of force sensing strategies are related either to passive or active technologies. Passive force sensors, as strain-gauges sensors, only require a power supply to feed the transducers, while active force sensors require an additional excitation on the test-body aside the to-be-measured force. In the case of resonant force sensors, the additional input is an harmonic excitation that allows tracking of resonant frequencies of the test-body. This mode of operation is similar to the operation of a guitar: tension in a guitar string can be estimated by measuring its resonant frequency, but to know such frequency (pitch) the guitar string must be excited. In resonant force sensors, transducers are used in actuating-sensing pairs. One of the transducers acts on the test-body to excite its mechanical resonance(s), and then another transducer picks up the signals. Piezoelectric patches are mostly used for actuating resonant sensors, [6, 56], because piezo-patches are easily integrated into the sensor structure. Piezo-patches are also suitable for sensing back the signals thanks to the piezoelectric direct effect (frequency shift can be measured on-line using dedicated Phase Lock Look (PLL) trackers, see Figure 2 on the contrary to others realizations that rely on external vibrometers laser [2, 19]). Resonant force sensors are used in a wide range of forces [37], from industrial applications with force sensors achieving 20 kN, [17], to microscopy where they achieve $< \mu$N, [28, 55]. They are widely used in microelectromechanical systems, as atomic-force microscope tips, [19, 41, 48]. Recent works on quartz crystal resonators present force sensor in the human range, [46].

Resonant sensors can be seen as Frequency Modulation (FM) generators. As an analogy with the FM radio transmission, the input signal is related to the to-be-measured force, or applied force, and the carrier signal is related to the resonant frequencies. A demodulation of the test-body response signal will give us back a signal image of the applied force. As their frequencies contain the information about the applied forces, signal amplitudes can be used to monitor sensor malfunctioning. This health monitoring option, can be used to prevent injuries to the operators in a robotic environment. Moreover, because signals provided by resonant sensors are constantly updated, creep phenomena are drastically reduced compared with strain-gauge-based force sensors.

As identified in the state of the art presented at the beginning of this paper, the study and development of resonant sensors mainly concern single axis measurement. Note in particular that single-axis resonant force transducers are not easy to design because their design requires multi-domain and multi-physics analysis. But the design of multi-axis force sensors is even more difficult. One of the hightlights of this paper is thus to propose for the first time a rational approach to design these multi-axis resonant force sensors. Standard resonant sensor test-bodies rely on beams as illustrated in [21]. One of the most used topologies for resonant force sensor is the Double Ended Tuning Fork (DETF), which presents very few energy losses, [4]. These loses define the quality factor (mcQ) of a sensor test-body because high-quality factor leads to high resolution and sensitivity [28]. Quality factor can be improved by a specific attention paid to the design of the test-body, or by using an evacuation cavity (reducing air damping), [27]. Other types of res-

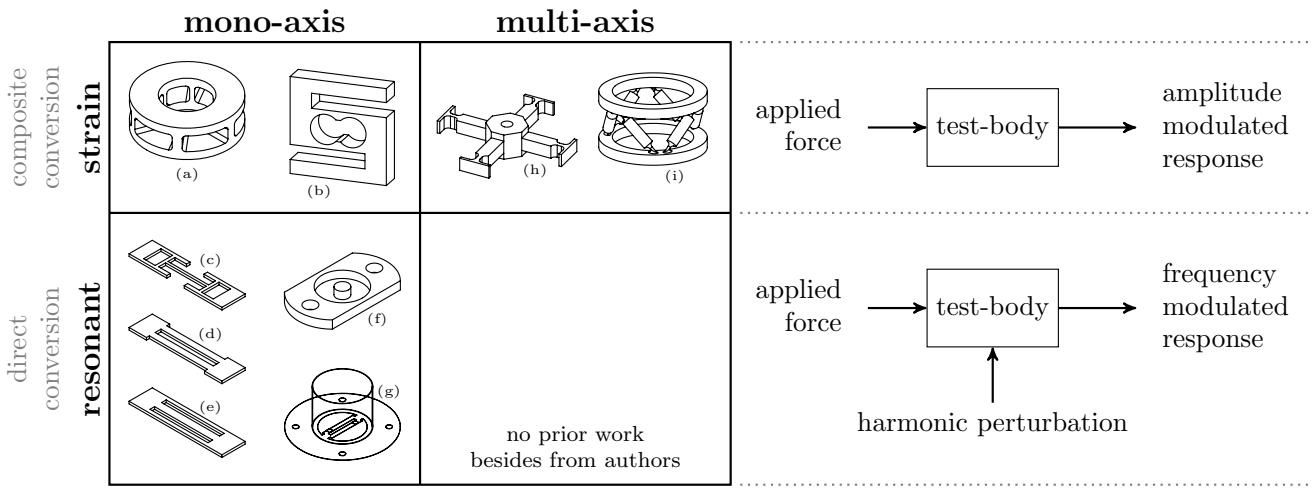

Figure 1: Grouped force sensors by its characteristics: number of sensitive axis and the sensing principle. It can be pointed out that, according to our knowledge, no multi-axis resonant sensors were proposed before our work. Different sensor test-bodies are presented: (a) one-axis hollow hexa-form torque sensor, [1], (b) s-form force sensor, [54], (c) single beam tuning fork, [27], (d) DETF, [6, 17, 28], (e) TBTF, [56], (f) out-of-plane membrane sensing element, [45], (g) DETF load cell structure, [4, 5], (h) Maltese cross shape, [15], (i) *Stewart* platform, [63]. On the right, we present a significant difference between the two types of test-bodies: resonant test-bodies receive an additional harmonic perturbation. Those test-bodies response is frequency modulated instead of amplitude modulated.

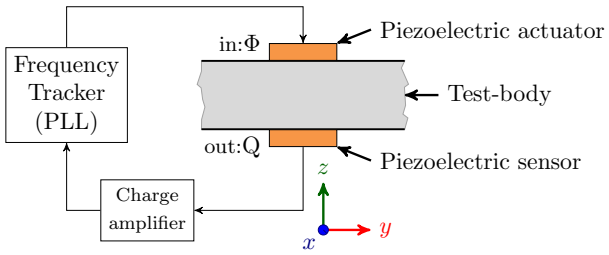

Figure 2: Frequency tracking principle: An harmonic excitation is send to the sensor test-body. Such electric potential excitation Φ is transferred as vibrating force to the test-body by a piezoelectric actuator. The test-body response is then captured by a piezoelectric sensor in the form of electric charge Q. This charge is conditioned, and the sent to the tracking unit.

onant sensors use the *Langevin* structure to measure applied forces. These sensors may increase the frequency bandwidth using stack piezoelectric elements with metallic counter-mass, [52, 62].

The main advantages of resonant force sensors over strain-based force sensors are the following:

- Force sensors are intended to be stiff and rigid. This requirement goes against the composite-conversion type force sensors, based on displacement measurements: rigid sensors of this type need therefore very high sensitive transducer elements to be effective. Resonant force sensors, or in general direct-conversion type force sensors, are not concerned with this limit specific to composite-conversion type force sensors.
- Strain-gauges force sensors present drift, and noisy signals. Such problems are minimized when using resonant sensors. [4] shows that increasing the mechanical quality factor will improve the noise rejection of the sensor, as well as its quality of measures.
- Resonant force sensors make it possible to retrieve two types of information from the test-body: amplitudes and frequencies of signals. Applied forces are estimated using frequencies. Then, amplitudes can be used for health monitoring of the sensor. In such a purpose, simple root-mean-square signal processing can detect failure or malfunction. Strain sensors do not have this option.

2.2. *Principle of Resonant Force Sensors*

Resonant force sensor test-bodies are mechanical structures whose natural frequencies and modal shapes are sensitive to an external force (named the to-be-measured forces $\mathring{F}$ in the sequel). Such force can be considered as a part of the boundary conditions of the structure. The sensing principle lies on the fact that frequencies and modal shapes of a structure are strongly dependent on their boundary conditions (force and/or displacement).

Let us explain this principle on the Figure 3. We consider an initial free-of-load test-body V, which has been pre-stressed ($\mathring{\sigma}$) by an external force $\mathring{F}$. In this new state $\mathring{V}$, set as the working point, a forced excitation is applied F^{exc}, using piezoelectric actuators. Such excitation drives the test-body into its resonance, which shifts according to the applied pre-stress force $\mathring{F}$. Two different kinds of forces are considered in these sensors, they differ by their frequency range:

$$\text{frequency of } \mathring{\text{F}} \ll \text{frequency of } \text{F}^{\text{exc}}$$

- The excitation force F^{exc} appears at high frequency. F^{exc} will be created with piezoelectric elements to excite the

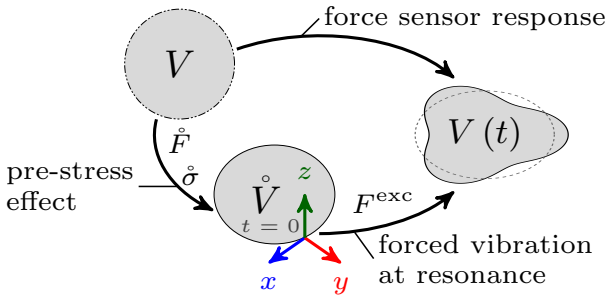

Figure 3: Force sensing principle: A pre-stress body volume $\mathring{V}$ is excited by a piezoelectric generated force F^{exc}, which puts the body into the resonance $V(t)$. The initial pre-stress $\mathring{\sigma}$ affects these resonances. Such pre-stress is created by the to-be-measured force $\mathring{F}$.

resonances of the structure. Resonances can be obtained by the application of electric potentials Φ to piezoelectric patch electrodes (as shown in Figure 2).

- The to-be-measured force $\mathring{F}$ appears at a relatively low frequency. In interactive robotics applications, the range of frequencies of to-be-measured force $\mathring{F}$ are far below the resonant frequencies of test-bodies. In such a case, they can be considered as *quasi-static* forces that only affect the mean strain of the test-body. The relation between the to-be-measured force $\mathring{F}$ and the frequency shift of the structure can be expressed using the mechanical pre-stress theory and exploiting by the signal processing of the sensor.

An accurate model of operation is required to efficiently design resonant sensors, whether single or multi-axis. This paper presents the overall design of the 6-axis F/T sensor as well as its performance and features. In order not to make this paper cumbersome, the precise dynamic modelling of the sub-elements (beams and plates) is not reproduced here but can be found in detail in the previous publications [11, 14].

Electronic tracking units are used with the test-body to retrieve the information about the resonant frequencies. Two different implementations can be found in practical applications. One configuration uses PLL circuit (example of the Figure 2, [12]). Other tracking systems are based on active instability triggering in test-body dynamics (triggering of limit cycles in the vibrations behaviours of test-bodies, [13]).

The vast majority of resonant force sensors concerns one-dimensional force sensors and are based on beams. Double Ended Tuning Fork (*DETF*) and Triple Beam Tuning Fork (*TBTF*) are the most common types. As displayed in Figure 1d, DETF structures have two parallel beams that are connected at both ends. DETF are suitable for tensile loads. For compressive forces, support structures, like columns, are required. Sizing of supports for DETF are detailled in [42]. This allows the application of force in the axial direction of the DETF, [17, 23].

An alternative design suitable for compressive loads uses two parts: a cylinder and a membrane with a DETF engraved (see Figure 1g). In this case, a compressive force stretches the membrane via the cylinder. This compact mechanical arrangement transforms the compressive applied force to a tensile force that is transmitted to the DETF, [5]. The cylindrical compression cell transmits the force uniformly to both beams, avoiding the configuration of unbalanced forces that could separate the structural dynamics into two distinct sub-dynamics (one for each beam) with different resonances, [26].

Typically this structure utilizes a resonant modes of beams in opposition of phase (180° phase shift). The use of such a mode is preferred when considering cancellation of the residual angular moment. This configuration reduces also the losses, [6]. Using flexural mounting at both ends of the DETF, the damping of the structure is reduced and, as a consequence, the quality factor increases, [4]. [18] proposes extensive experimental results to quantify the influences of dimensions and parameters on DETF behaviour for improving their performances. Currently, Double beams force sensors have achieved mcQ-factor up to 150 thousand.

Triple Beam Tuning Fork (*TBTF*) structures present three parallel beams (see Figure 1e). The TBTF uses generally anti-symmetrical out-of-plane bending modes that inherently cancel the moment at the ends, [27, 64]. One example of application uses the center beam to measure out-of-plane force using a specific mode where the outer beams vibrate in opposition of phase and the central beam remains free of vibration, [22]. One advantage of TBTF over DETF is the higher sensitivity, but they present a reduced quality factor. The double and triple beam configurations increase the mcQ-factor of the resonant structure by cancelling the moment at the base point, encapsulating the energy.

As confirmed by our recent literature review, there is few works on membrane or plate structures for force sensing ([29] describes one of the few references identified on this topic). [45] presents a membrane designed for measuring a non-contact force in the out-of-plane direction (see Figure 1f). This design uses a permanent magnet on the membrane and a coil to generate an electromagnetic force.

One of the main purpose of this paper is the design of resonant structure sensitive to more than one axis of force. The total number of sensitive elements for multi-axes sensors are then reduced. Plates (two-dimensional) are the logical extension of beams (one-dimensional element) and we consider in the following the plate as the suitable candidate for being the elementary sensitive element for multi-axis (or multi-degrees of freedom) resonant force sensors.

3. Multi-Axes Resonant Force Sensors

Building a multi-axis resonant force sensor requires a complex design stage. This design should meet several drastic constraints from different scientific areas: modal frequency analysis, vibrations, mechanical structures, and control. The design is hardly manageable in one step but several, firstly focused on the sensitive elements, then on the whole sensor structure. In

this context, the sensitive elements can be seen as independent modular parts of a full wrench estimator.

Multi-axis implementations of resonant force sensors are unusual, due to the difficulty to deal with its non-intuitive dynamical behaviour. A recent review of the literature has not shown any functional example of this type of device except the one presented in this paper, either at the industrial level or at the research laboratory level. Recent papers in the field proposes some preliminary resonant-based prototypes for measuring forces up to 50 N [58] , or even up to 1500 N [50]. However, they rely on preliminary designs that lead to only one single axis force measurement as a main limitation. At the micro-scale force measurement, very few attempts have been revealed in the literature to extend the resonant principle to the multi-axis case: they are still restricted to a very limited number of degrees of freedom due to the difficulty to account for several modes of resonances in the MEMS sensor design [19], while the shifts of the resonant frequencies are often still measured with external means out of the sensor, such as laser vibrometer.

Actually, the design of resonant multi-axis sensing devices needs to take into account modal-based considerations. In this section, we present first the guidelines for designing resonant sensors. A simple inexpensive, but efficient enough, resonant smart structure is then proposed for measuring three components of an externally applied force. This smart structure will be extended in the next section for estimating a full wrench (3 forces and 3 torques).

The best way for designing multi-axis force sensors is to address it as an optimization problem with constraints, [9, 40]. Nevertheless, due to the complexity of the design problem, we focus initially on the search for admissible solutions. The search for an optimal solution can only be considered in a second step, when it is shown that admissible solutions exist and that their performances are not sufficient with respect to the expected requirements. We consider in a first step the following requirements: exceeding the current best performance of resonant sensors (precision, dynamics) and being usable (integration, robustesse, safety) for collaborative robotic applications. There are three main guidelines for sensor design. Two of them are set as objectives ($\mathbb{O}_1$ and $\mathbb{O}_2$):

$\mathbb{O}_1$ The increment of sensitivity $\|S\|$ (useful for all sensors) [43, 44].

$\mathbb{O}_2$ The reduction of the calibration matrix's condition number N_C (for multi-dimensional or multi-axis sensors), [7].

The third guideline, specifically dedicated to resonant sensors, is set as a constraint ($\mathbb{C}_1$):

$\mathbb{C}_1$ The frequency clearance (actually, this is the main constraint for resonant sensors), [24].

Resonant sensor design is not intuitive because of the coupling between all its design parameters. These parameters are the test-body material, the plate dimensions (width, length and thickness) and the dimensional parameters of the other mechanical elements. Let us define the general objective function $\mathbb{O}_G$ that expresses the design problem in terms of an optimization problem. This objective function mixes the two previous objectives into one simple fitness function by setting the general objective to maximize the ratio between the sensitivity $\|S\|$ and the condition number N_C : $\mathbb{O}_G = \|S\|/N_C$. The sensitivity relies on amplitudes of the measured signals. The condition number limits the estimation errors. Each one of these two objectives has been considered as the objective function when optimizing sensor designs. Some consider the condition number as the objective function to minimize, [7]. Others consider the sensitivity as the function to maximize, [43, 44]. In addition, some particular constraints come from current manufacturing capabilities and from the resonant nature of our device. Finally, the optimization problem reads as: *find the design parameters that maximize $\mathbb{O}_G$, respecting the constraints $\mathbb{C}_1$.*

3.1. Resonant Sensor Design Guidelines

Sensor sensitivity characterizes the relationship between natural frequency and applied forces (see Figure 4). The sensitivity is the slope of the curve of resonance frequency shift according to applied force. Sensors with high sensitivity present two advantages:

- Small variations in the force input (called the *mesurand* when it is the physical quantity to be measured) create large variations in the frequency signals (measure). It is easier to detect small force changes in high-sensitivity sensors.
- At the contrary, small variations on the measure (like noise) do not affect the estimation of the force (noise in the measure represents negligible force variations on the estimation).

These characteristics show the importance of increasing the sensitivity of the sensor ($\mathbb{O}_1$). The sensitivity needs to meet a major constraint:

$\mathbb{C}_2$ sensitivity curve needs to be a one-to-one map, i.e. a bijective function. This condition enables the inversion of the sensitivity curve, which is necessary to estimate the input force.

Estimating the different components of force requires the measurement of several frequencies. Number of measures m must be equal to, or greater than, number of components of the to-be-measured forces (6 at the maximum). The calibration matrix $[C]$ captures the relationships between forces and frequencies. It is the inverse (or *Moore-Penrose* pseudo-inverse for $m > 6$) of the sensitivity matrix $[S] = \left[C^{\dagger}\right]$ of the sensor. Nevertheless, this calibration matrix exists only for sensors with linear characteristics because it assumes a linear mapping between forces and frequencies.

$$\{F\} = [C]\{\Delta f\} \qquad \begin{cases} F \in \mathbb{R}^6 \\ \Delta f \in \mathbb{R}^m \end{cases} \text{ with } m \geq 6$$

The condition number N_C of this matrix informs on the performances of this sensor. Reducing this number reduces the

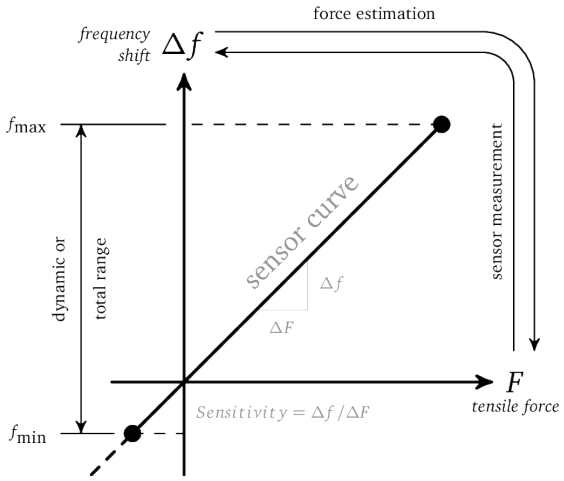

Figure 4: Sensitivity of a resonant force sensor.

upper bound of the error propagation factor K_p, [7, 32]. Propagation factor limits the errors on estimated forces and is defined as:

$$K_p(C) \leq \frac{N_C}{1 - N_C \epsilon_C} \tag{1}$$

with $N_C = \|C\| \|C^\dagger\|$ the condition number. ϵ_C is the relative error on the calibration ($N_c \epsilon_c < 1$ is assumed). Relative error on the force estimation ϵ_F can be computed knowing this propagation factor:

$$\epsilon_F = (\epsilon_f + \epsilon_C) K_p(C) \tag{2}$$

where ϵ_f is the relative error on the frequency measure. Decreasing the condition number improves the sensor design, by limiting the force estimation error, then allowing simpler estimation algorithm and signal processing.

Resonant force sensors rely on the relationship between frequencies and forces. This relationship should be, at least, one-to-one and, as much as possible, linear in a region of interest. These good properties ensure a linear characteristics of the force sensor.

It is worth noting that when two different mechanical resonant frequencies are close, their modes interact and mix. This interaction affects also the phase of damped structures, especially near resonances. When phase response does not follow a local bijective function, frequency tracking is not possible and the measure of the frequency is no longer valid, [24]. This explains why design of vibrating structure has to take into account the frequency clearance $\mathbb{C}_l$ as main constraint. We can say that a frequency range has frequency clearance when two conditions are satisfied:

1. The region is free of spurious modes (a spurious mode is an unexpected and undesirable mode).
2. The frequencies of interest within the region are far from the other, and can be well-distinguished.

Figure 5 (a) shows an example where the interesting resonances are close to spurious resonances, [26]. The spurious resonances

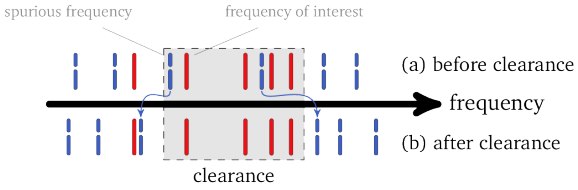

Figure 5: Principle of the frequency spectrum clearance. "Spurious" resonances of the plate structure are in blue and sensitive resonances, i.e. usefull resonances, are in red. The spectrum before clearing represents the first iteration of the prototype, when some of the resonances of interest are affected by spurious resonances coming from the *test-body* structure. The cleared spectrum (after clearance) corresponds to the final prototype and its dynamic behaviour.

are those who present a modal shape with a non-negligible motion outside the plate. Without clear zones, the sensor may fail to work properly, as non-linear and unpredictable behavior appears. Figure 5 (b) shows the resonances of a prototype which has a cleared zone. This zone presents four resonances of interest that correspond to predictable behavior. This makes them suitable to be used in a closed-loop tracking system. It must be stressed that these four resonances can be exploited to estimate the three components of force only because corresponding frequencies are distinct and far from each other. Very close frequencies/modes generate tracking problems because the shape and the phase of one mode is affected by its nearest neighbor. This causes crossing effects and the tracking system fails.

3.2. *Design of a 3D Prototype*

As mentioned in the introduction, this paper concerns the design of a 6-axis force sensor (3 forces, 3 torques), the presentation of its signal acquisition and processing system as well as an experimental verification of its performance. However, this 6-axis sensor is based on an arrangement of several 3-axis sensors that only measures forces and not torques. This basic 3-axis sensor is the result of previous works by the authors and, as such, has already been published in [11, 14]. Thus, only some essential elements of these previous publications are reported below.

This basic 3-axis sensor allows the simultaneous measurement of 3 components of force using a single test-body (see Figure 6). Different configurations have been studied and a design has been finally chosen for experimental validations. To scale the three components of force, a monolithic structure has been designed as test-body. It consists of a vibrating force-sensitive plate and a massive mechanical frame which acts as a clamping system in the range of the resonant frequencies of the plate (displacements are prevented while the structure is operating dynamically at high frequencies). The mechanical frame is fixed at one corner, while a static external force $\mathring{F}$ is applied to the opposite corner. This force is effectively transmitted to the force-sensitive plate through the mechanical frame.

The placement of the transducers plays an important role in the design of the resonant sensor. The ability of a particular piezoelectric actuated (or sensing) patch configuration to

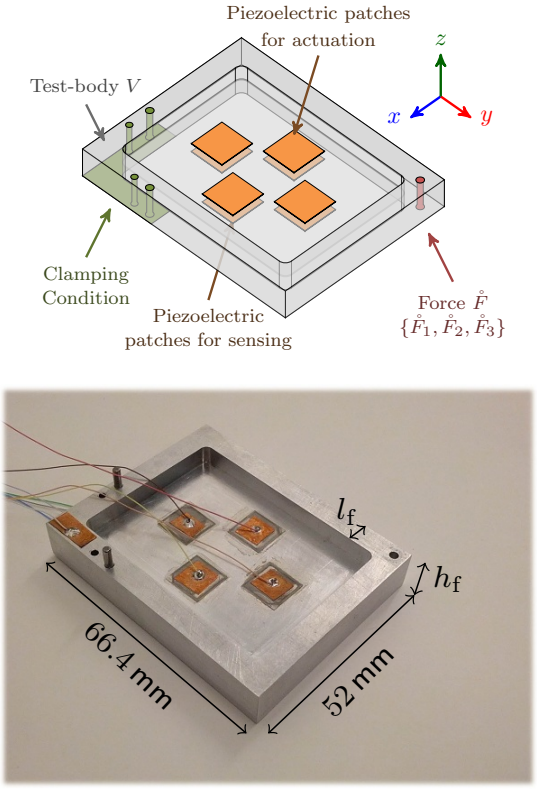

Figure 6: Multi-axial resonant force sensor test-body description: it is composed of a plate ($40 \times 54.4 \times 0.5$ mm^3), a frame ($l_f = 6$ mm made of aluminium and $h_f = 10.5$ mm) and eight piezoelectric patches (PIC151 of dimensions $10 \times 10 \times 0.2$ mm^3), four in the upper side for actuation and four in lower side for sensing. The bonding of the patches is ensured by a conductive paste from *EPOTEK* company.

control (or to observe) a resonant frequency of the plate is directly linked to its relative placement to the nodal lines of each mode. Thus, the patches placement on the nodal line of a selected resonant frequency of the plate leads to insensitivity to such mode, and acts as a "spatial modal filter". The principle of modal spatial filtering applied to this basic 3-axis force sensor is explained in depth in [12].

To characterize the basic 3-axis force sensor, a test-bench has been designed (see Figure 7). It allows us to apply a force and to measure it via a external calibrated force sensor (*Futek*). The application of force can be oriented within a range of about 90° in a plane parallel to the plate and 90° out-of-plane. The test-bench integrates potentiometers at the axis position for precisely measuring the force application angle (to decompose the to-be-measured force $\mathring{F}$ into the three components of force $\mathring{F}_x$, $\mathring{F}_y$ and $\mathring{F}_z$). In addition, the test-bench also integrates a laser sensor device *Keyence* to identify the modal shape of each resonance of the structure.

The whole prototype of the the basic 3-axis force sensor including the instrumented sensing plate system, the controllers and the signal conditioning elements have been implemented using analog electronics exclusively. The signal conditioning elements are built by addition and subtraction circuits using operational amplifier arrangements. The use of analog electronics allows a very large bandwidth. Figure 8 presents the wiring of the prototype and the control units. After sensing, a signal conditioning is realized before actuating the prototype. An analog electronic extracts a signal proportional to the resonant frequency. Each control unit provides a resonant frequency. The information about the calibration sensor, the angular measures, and the resonant frequencies measurements are recorded and processed in the data acquisition unit.

The mapping $\mathring{F} \rightarrow \Delta f = f - f_{\mathring{F}=0}$ has been identified experimentally. The complete experimental protocol of this identification procedure can be found in our previous publications [12, 14] concerning this basic 3-axis sensor. In Figure 9 the estimated forces are compared with the measures of an external *Futek* force sensors. The time recording of measurement signals permit to expose the interesting properties of our prototype in terms of accuracy (small relative errors between both force estimations), bandwidth (no perceptible lag effects) and axis decoupling (i.e. the cross-coupling effects effectively taken into account through the calibration matrix) for a wide range of force.

The tests were made in a range of force of 50 N in each axis (given by the limit of the calibration sensor). However, plate structures are designed to support up to 300 N without damage. This smart sensor can actually estimate three components of force with an accuracy of nearly ±1 N for a force range of 50 N which corresponds to an accuracy of ±2%. This is enough for collaborative manipulation tasks, [25, 57].

A second version of this 3D force sensor was proposed to enhance its characteristics and performances. The ratio $r_a = \frac{b}{a} = 1.36$ between its length b and width a was optimized for increasing its sensitivity (Figure 10 a). A plate offset in the Z-direction was adopted to enable a one-to-one characteristics in the Z axis. Finally, the frame topology was modified to improve the frequency clearance (Figure 10 b)). The final topology of this sensor is reported in the Figure 11. The comprehensive description of the tracking command of this basic 3-axis sensor having already been published in [13], it will not be reported again here.

Different design strategies have been used for designing this smart structure, e.g high-frequency clamping, spatial modal filtering, and selective modal signal conditioning. Smart structure, electronic instrumentation and control together allow the manufacturing of a sensing system that is capable of estimating all the three components of force, by measuring superimposed resonant frequencies shifts, using an intelligent extraction algorithm.

This structure will be extended in the next section for proposing a full wrench sensor. Note that compared to this first 3D prototype, the 6D Full Wrench prototype that will be presented in the next section uses 12 circular piezoelectric patches on each resonant plate instead of 8 square patches (see the corresponding configuration in Figure 14). This modification has improved the overall performance of the sensor in terms of accuracy and detectability of different modes compared with this first version.

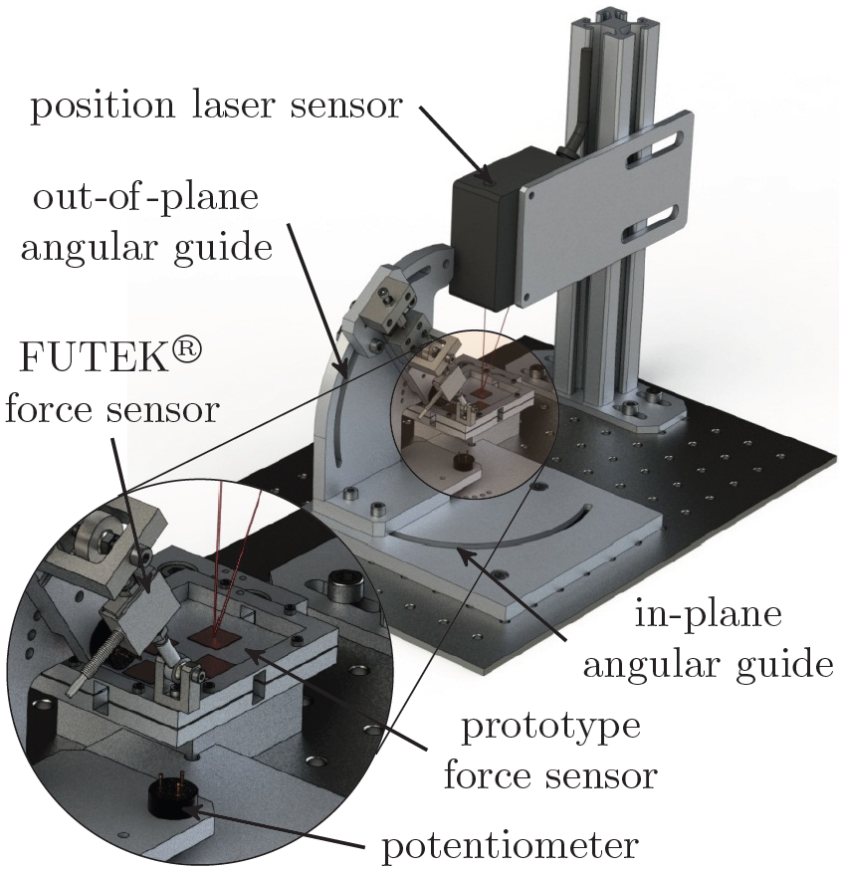

Figure 7: Experimental setup to validate the basic 3-axis force sensor. The test-bench is placed on an optical table. The sensor prototype is clamped via a fixation element to the table. The force is applied to the prototype via a calibration sensor (*Futek* LSB200) with a force range of ±50N. This sensor only measure the force on its axial direction. To obtain the information of the three components of force, two angular sensors are added. The application of force is made manually. A laser position sensor helps us to determinate the modal shapes of the different resonant frequencies [12].

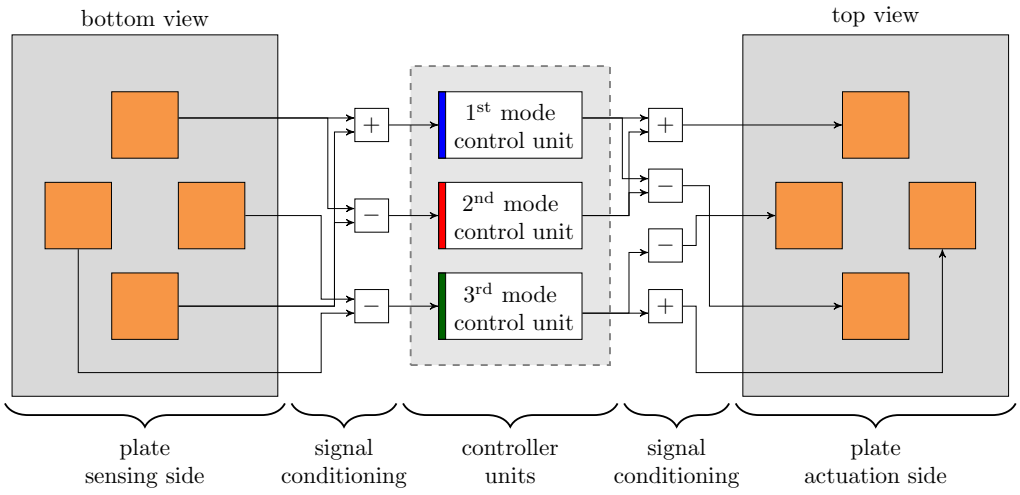

Figure 8: Electronic wiring between the control units and the prototype piezoelectric patches. The signal pass trough different signal conditioning elements. Details on the control methods and the signal conditioning can be found in [12, 13].

4. Full Wrench Resonant Force Sensor

As noticed previously, there are two well-known structures in the domain of six-axis strain-gauge force sensors (non-resonant force sensors). These structure are based on beam as seen in the Figure 12: *Maltese* cross, [34], *Stewart* platform, [61, 63]. The *Maltese* crosses present 3 or 4 beam sensitive elements.

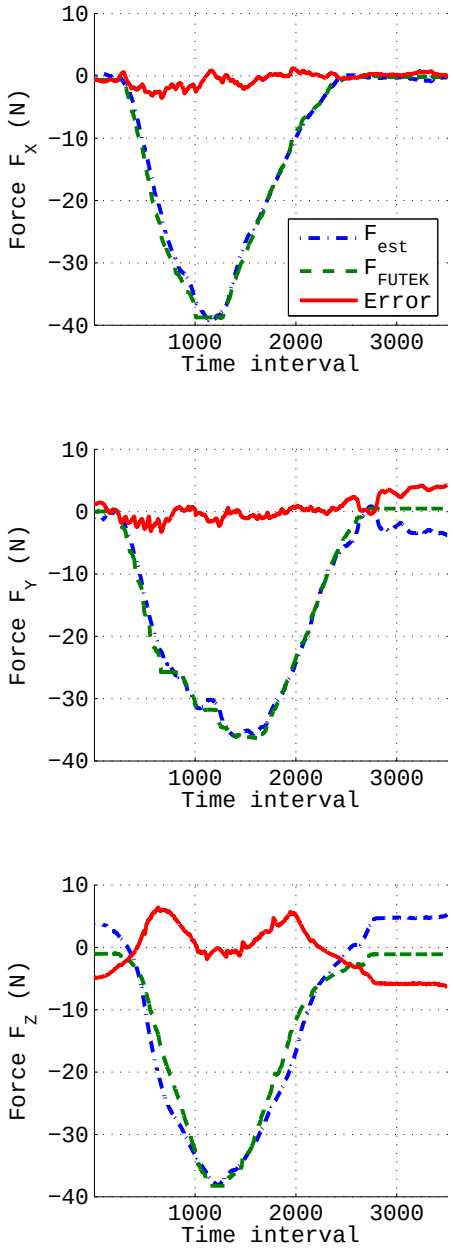

Figure 9: Comparison between the estimated force using the prototype sensor, and the applied force, retrieved from the calibrated *Futek* sensor. The time interval is presented in milliseconds. The error on the estimation of F_z around 2500 ms can be due to multiple factors: the test-bench response on the z-direction, a non-linearity in this direction and, a bad zeroing of the F_z offset. Forces are given in Newton (N) and time interval in second (s).

Each beam is sensitive to more than one axis of force. The *Stewart* platform has 6 beam elements that are sensitive to one force only. Beam resonators could replace the Stewart platform beams, [31]. The manufacture of the second sensor structure is arduous. Such structure embeds flexible or spherical joints on the beam ends. They serve to decouple and increase the beam sensitivity along its own axis.

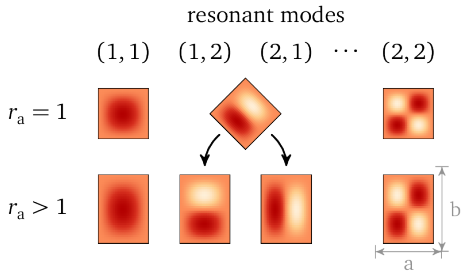

(a) Mode shape of the test-body according to the size ratio

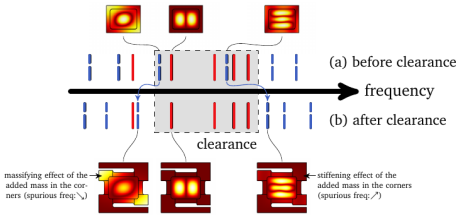

(b) Frequency clearance of the improved test-body

Figure 10: **(a)** Mode shapes of the test-body according to the shape ratio $r_a = \frac{b}{a}$ with b the length and a the width of the resonating plate. **(b)** Frequency clearance before and after the improvement of the test-body.

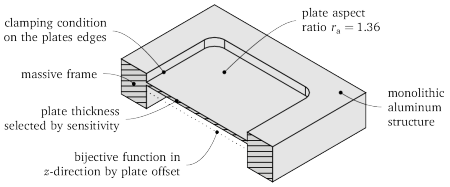

(a) Design parameters of the test-body plate

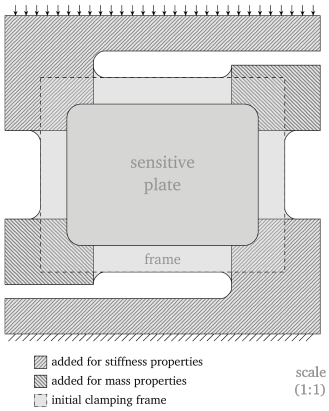

(b) Improved topology of the structure

Figure 11: **(a)** Design of the plate. **(b)** Topology of the improved 3D force sensor (plate + frame structure).

4.1. Additional Design Guidelines for Wrench Sensors

Our full wrench resonant force sensor embedds several previously designed sensitive elements (3D plate-based force sensor). The design of this 6-axis wrench sensor also seeks to satisfy the objectives $\mathbb{O}_1$ and $\mathbb{O}_2$ and to respect the constraint $\mathbb{C}_1$. In addition, the test-body design must take into account four

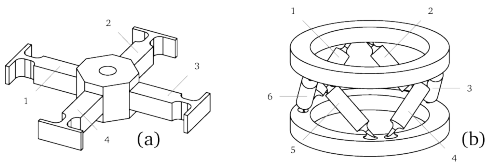

Figure 12: Representation of beam-based *test-body* structures. The presented sensors can estimate the six components of the force wrench. (a) This *Maltese* cross has 4 sensitive beams, [15]. (b) The *Stewart* platform has 6 sensitive beams, [63].

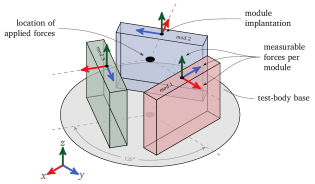

Figure 13: Sensitive elements placement on the test-body base (inspired from [33]).

additional rules:

- $\mathbb{R}_1$ **Modularity:** The sensitive element is considered as a module for designing the test-body, i.e. the test-body implements several modules (sensitive elements).
- $\mathbb{R}_2$ **Rotational symmetry:** The placement of the sensitive elements follows rotational symmetry because it offers a good condition number ($\mathbb{O}_2$) to the calibration matrix of the whole six-axis sensor.
- $\mathbb{R}_3$ **Uniqueness:** The use of identical sensitive elements has the same effect as having identical dimensions of a plate: it creates repeated resonant frequencies on the test-body and interference phenomenon between them. The use of different thickness on the sensitive plates separates these resonant frequencies, ensuring the meeting of the constraint $\mathbb{C}_1$. An optimization process of the thickness of the plates will separate them as far as possible.
- $\mathbb{R}_4$ **Redundancy:** We can use redundant measurements to improve the design. Adding *new information* about the applied forces reduces the condition number ($\mathbb{O}_2$).

4.1.1. *Modularity* - $\mathbb{R}_1$ *: From a Module to the Whole Sensor.*

A modular design approach presents many advantages

- Simplify maintenance.
- Increase performance.
- Creates homogeneity.

Figure 13 shows the placement of the three modular sensitive elements. Three sensitive elements are the smallest number of modules and the ideal number to ensure the estimation of the force wrench. Having more modules in a parallel configuration increase the stiffness and reduces the sensitivity (it goes against the objective $\mathbb{O}_1$).

4.1.2. *Rotation Symmetry* - $\mathbb{R}_2$.

The placement of the three sensitive elements in the test-body follows a rotational symmetry. They are distributed along a circle and separated by an angle of 120° (Figure 13). The size of the sensing element defines the radius of this circle which must be as small as possible. The use of rotational symmetry in the design should improve the condition number of the calibration matrix since rotation matrices have a unit condition number. This rotation homogenizes the sensitivity in the plane perpendicular to the axis of rotation. The condition number is invariant per rotation. Adding more sensitive plates will not reduce this condition number.

4.1.3. *Uniqueness* - $\mathbb{R}_3$ *: Avoiding Multi-Plate Interference.*

The test-body may have repeated resonant frequencies if we use several identical sensitive elements. Repeated resonant frequencies may interfere between them. Cloning the sensitive elements on the entire sensor is not desirable. The frequency clearance ($\mathbb{C}_1$) forces us to make variations in the plate parameters. For our three-module design, we choose to differentiate the sensitive element plates only by changing their thickness. This slight modification changes the resonances and leaves the whole structure as symmetrical as possible (necessary for the rotation symmetry $\mathbb{R}_2$). The use of different thicknesses on the sensitive plates separates the resonant frequencies: variations of 30 μm is enough to separate the frequencies as needed.

4.1.4. *Redundancy* - $\mathbb{R}_4$

Estimating the whole force wrench ($F \in \mathbb{R}^6$) requires at least six measures. Measuring more frequencies than required creates redundancy on the measurements. When the redundancy adds new information, it reduces the condition number ($\mathbb{O}_2$). But, if the redundancy does not add *new information*, this could increase the condition number and could increase the error propagation factor. Redundancy can be achieved by adding more sensitive elements, but, this increases the stiffness (in a parallel configuration) and reduces the sensitivity of each element because the sensitivity is divided by the number of sensitive elements when they are placed in parallel. This goes against the objective $\mathbb{O}_1$. Including more frequency measures per sensitive element is the better way to increase the redundancy without decreasing the sensitivity. The Table 1 shows which configurations allow us to estimate the entire force wrench. From this test-body design, twelve resonance frequencies are available, four per sensing element. We will use them all (the twelve) to exploit redundancy.

Note that in order to measure 4 frequencies per sensitive element without being troubled by modal filtering problems, we have adopted a configuration with 12 circular piezoelectric patches instead of 8 square patches as shown in figure 14. For the full wrench force sensor, the use of 12 patches allows to increase the sensitivity to more frequencies than in the 8 patches configuration.

Number of estimated components

Sensitive Elements	Measures per element			
	2	3	4	$\cdots$
1	2	3	3	3
2	4	6_S	6_S	6_S
3	6_M	6_R	6_R	6_R
4	6_R	6_R	6_R	6_R
$\vdots$	6_R	6_R	6_R	6_R

Table 1: Number of estimated components of the force wrench. This number depends on the number of measured frequencies per sensitive element and the number of sensitive elements. When considering two sensitive elements a *Special* issue appears (6_S). The use of two sensing plates and the measurement of three frequencies per plate allows the six force components to be estimated, but this configuration would not allow a torque to be measured that is aligned with the line that crosses the reference point of each sensing element. We have a *Minimal* sensor when considering three sensitive elements and two frequency measures per element (6_M). Using higher number of measures and sensitive elements generates *Redundancy* (6_R).

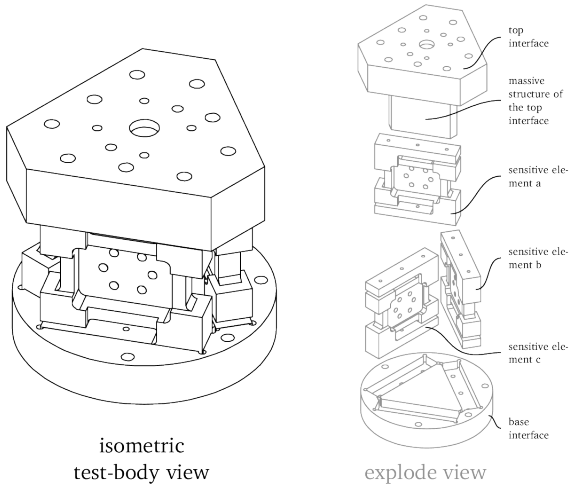

Figure 14: Entire test-body design. It comprises three sensitive elements, that are sensitive to the three components of the force. The entire test-body is then sensitive to the six components of the force wrench. Besides the sensitive elements, the test-body presents two interfaces. Those interfaces connect the sensitive elements between them and connect the sensor test-body to the surroundings.

4.2. Wrench Sensor Design

The other elements of the test-body serve as connections between the sensitive elements. They also serve as interfaces to fix the sensor and to apply the force wrench (see Figure 14). We design these elements considering always the frequency clearance constraint ($\mathbb{C}_1$). The top interface presents a massive structure to stiffen some twisting modes keeping them away the frequency range of interest. Our design has followed all the guidelines: it has a high sensitivity ($\mathbb{O}_1$), it presents a low condition number ($\mathbb{O}_2$) and it presents a frequency clearance ($\mathbb{C}_1$) in the selected frequency region. The different thicknesses of the plates are crucial to ensure the frequency clearance. Computer-assisted simulations have been continuously used for the design of the test-body.

The following paragraph summarizes the main concerns and solutions found to design our full wrench force sensor:

- Our sensor prototype was designed to be a multi-axis resonant force sensor for robotic applications. As noticed previously, there are no other multi-axis piezoelectric resonant force sensors reported in the literature that simultaneously measure 6D wrench components in a range of forces and torques that are compatible with the requirements of collaborative robotics. To fill this lack, we have first designed a plate-based resonant structure sensitive to three components of force. Then, we design a multi-axis wrench/force sensor built from several three-axis force sensitive plate elements (see Figure 14). Each plate exploits several superimposed resonant vibration modes. These resonances encode the applied forces as frequency modulated signals.

- The prototype working frequencies have been selected to maximize the relative sensitivity of the sensor in front of the applied forces. The placement of the piezoelectric elements generates a selective filtering of the signals that, combined with a smart signal conditioning, separates the frequency information of the different modes into multiple channels. The sensitive element plate has been enhanced with a structural frame that works as a clamping element. In addition, it also allows the sensitive element to have a bijective behavior over the three components of force. The frame makes the sensitivity to the out-of-plane force component bijective by allowing to have an offset of the plate from the frame middle plane (the other two force components are already bijective). This one-to-one correspondence is necessary for estimating the applied forces.

- The prototype has three sensitive elements and two connecting interfaces. Each sensitive element differs from the others by its thickness of the inner plate. Each one came from a single block of aluminum processed using classical milling. The final thickness of the plates are 441 μm, 491 μm and 510 μm. We use FEM analysis to optimize the separation of the frequencies between the 3 different plates. With a 30 μm difference in thickness we separate the same mode frequencies enough to avoid frequency interference and to be separated also from other modes. The initial objective is to have the thickness separated by 30 μm, but the manufacturing process ends up with the reported thickness. The choice has finally been made considering the manufacturing capabilities. The plate has twelve piezoelectric patches. Six patches are bonded to one side serving as actuator. The other six are bonded to the other side serving as sensing elements. The patches material is *PIC181* from PI, they are discs with dimensions $\oslash 5 \times 0.2$ mm.

The next section is devoted to the validation of this full wrench force sensor. Its performances are measured and compared to those of a industrial 6D sensor in a standard configu-

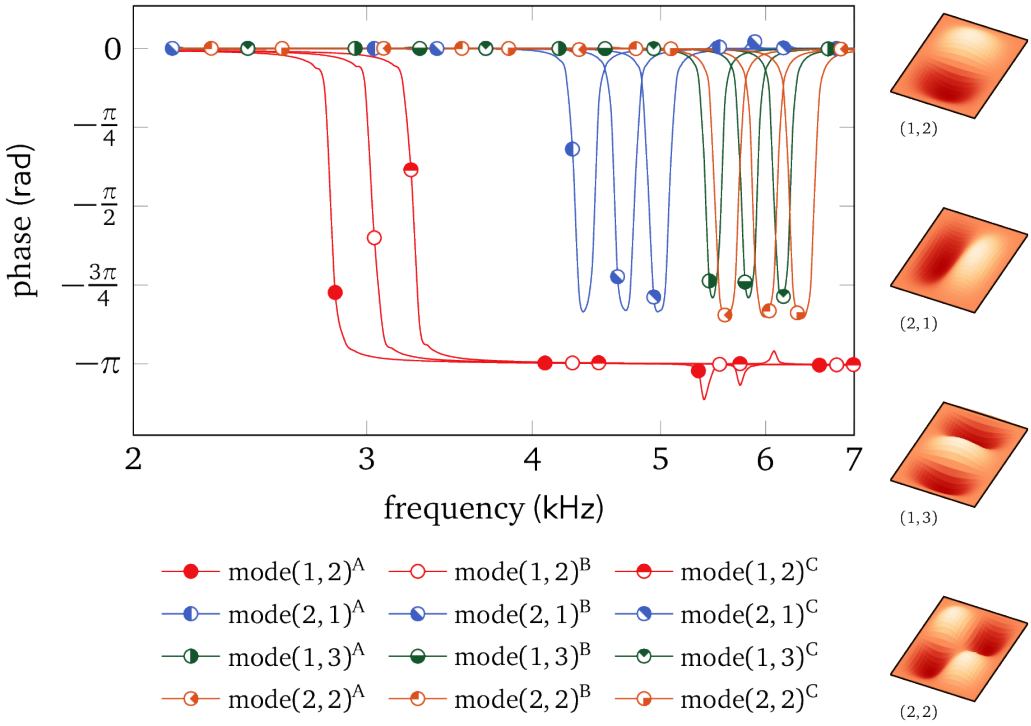

Figure 15: Phase responses of the entire test-body design. The figure shows the phase response of the four modes (i, j) of interest for each sensitive element plate A, B and C.

ration for collaborative robotics (force measurement in a robot wrist).

5. Validation of the Wrench Sensor

In a first step, we measure the frequency response functions of the three sensitive elements refered as A, B and C to validate the frequency decoupling of the full sensor prototype. The piezoelectric actuation is considered as input and the charge measurement as output. The process is repeated for each pair of actuating A_i and sensing S_i patches. The results, reported on the Figure 15, show that each signal (of each tracking unit and sensitive plate) has one single frequency in the region of interest (2 kHz–7 kHz). It also shows that the others frequencies are highly filtered. They are even hidden within the noise (-40 dB$\approx \pm$12 mV).

In a second step, a characterization of the full wrench sensor is made using a calibration sensor. Then, we perform a validation of the prototype by estimating the applied force using the identified calibration matrix. These estimations are compared with the calibration sensor. For these two experiments, a different setup is used based on the test-bench described in the Figure 16. The sensor prototype is placed on an anti-vibration table and attached through a connector to a calibration sensor. This calibration sensor has a handle that is used to apply manually the forces to the sensor by an operator. This configuration will allow to perform the calibration of the prototype sensor, and to validate its behavior.

The procedure of the experiment is presented in the Figure 17. The handle serves as an interface between the operator and the sensors. We can apply the different components of force using this handle. The applied force on the test-bench modifies the output signals of the sensors. These signals are conditioned by different electronics. The calibration sensor is an *ATI Delta* SI-660-60 sensor with a force range of 660 N. For this comparison, an *ATI Gamma* force sensor with a range of 100 N could have been a more interesting alternative, since it has a measurement range closer to our prototype and closer functional and non-functional characteristics. However, we did not possess this sensor, so we decided to use the *ATI Delta* which remains a relevant comparison sensor. Both force sensors are gathered using Labview and ADC on a real-time computer. It allows online signal processing. We also use Labview of a host computer for the interface. This interface is illustrated in the Figure 18. The host computer also embeds the calibration matrices of the prototype sensor and calibration sensor. With these matrices, the computer simultaneously estimates the applied force.

To calibrate the prototype sensor, we applied different sets of forces to the test-bench via the handle, following a trajectory imposed by the operator. The signals from both sensors are transmitted to the acquisition unit that converts these signals and sends them to the computer. The force application follows a force profile, while the computer records the frequency shift and forces simultaneously. The calibration sensor gives the information about the applied force (characteristics of the calibration sensor are reported in table 2). The prototype sensor gives the information about the frequency shifts. We can create

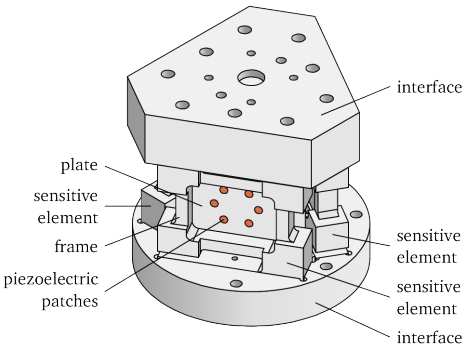

(a) Wrench force sensor prototype

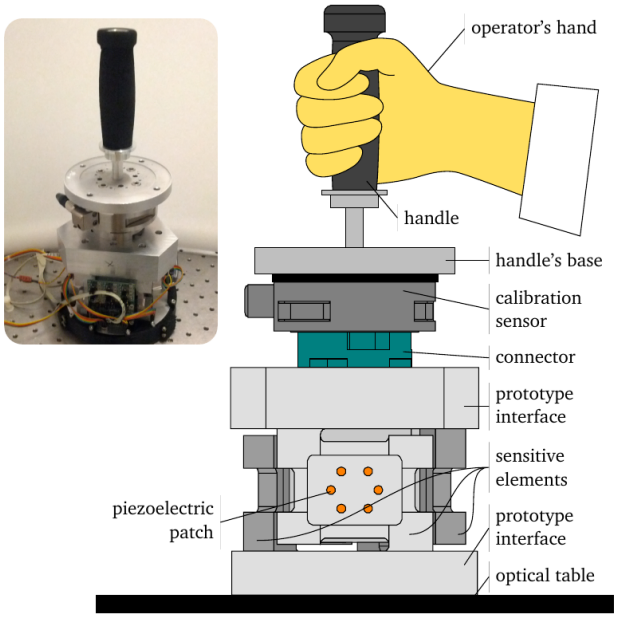

(b) test-bench

Figure 16: Experimental validation of the sensor: (a) Sensor prototype, (b) Test-bench for the sensor prototype characterization.

	range N or Nm	resolution N or Nm	overload N or Nm	stiffness N/m or Nm/rad	resonance Hz
F_x, F_y	±660	0.25	±3400	$37 \cdot 10^6$	1500
F_z	±1980	0.5	±12000	$61 \cdot 10^6$	1700
T_x, T_y	±60	0.015	±220	$52 \cdot 10^3$	1700
T_z	±60	0.015	±420	$94 \cdot 10^3$	1500

Table 2: Calibration sensor characteristics: *ATI Delta* SI-660-60

a mapping between these two quantities, $\mathring{F} \rightarrow \Delta f = f - f_{(\mathring{F}=0)}$. The sensitivity matrix stores the relationship between the quantities.

Considering the linear behavior of the prototype sensor, the relationship between frequency shifts $\{\Delta f_i\}$ and the to-be-measured force components $\{\mathring{F}_j\}$ is:

$$\{\Delta f_i\} = [S]\left\{\mathring{F}_j\right\} \quad \text{with, } i \in \{1,..,12\} \text{ and } j \in \{1,...,6\}$$

The pseudo-inverse of the sensitivity matrix $[S]$ creates the

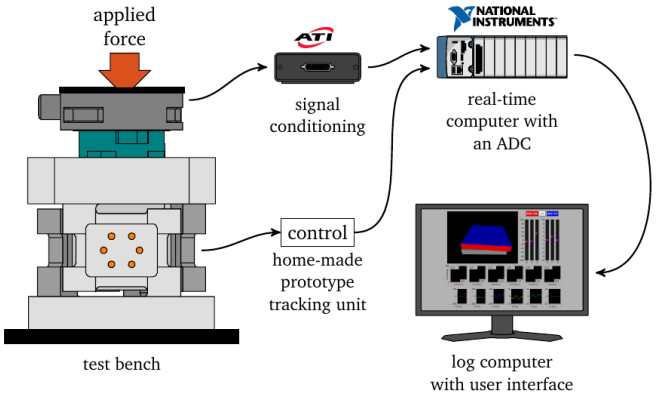

Figure 17: Setup for the calibration and validation of the sensor prototype. We apply forces on the test-bench that will change the physical properties of the two sensors. Their signals are treated by their respective signal conditioners. For the calibration sensor, it comes with a signal conditioner, and for our prototype, we use our tracking electronic card. Both controllers have an analog output, those are sent to a real-time computer that performs the analog-to-digital conversion (ADC). This computer is linked to a log computer with a user interface.

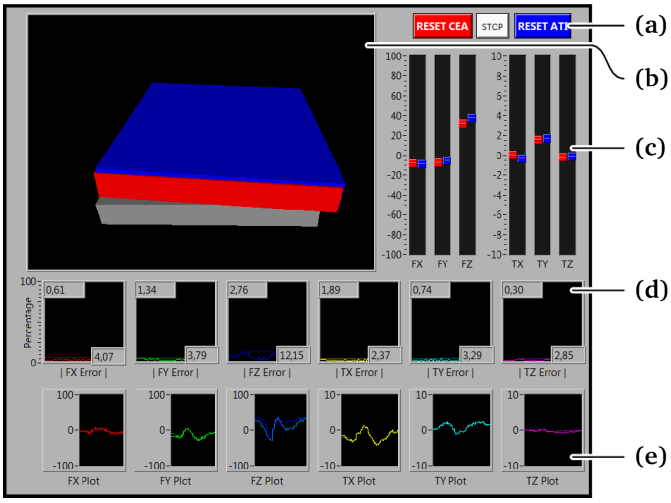

Figure 18: Computer interface. The interface has five different zones: **(a)** the control buttons, one button to stop the interface, and two buttons to initialize each sensor. **(b)** A 3D representation of the sensor forces, the red block represents our sensor, the blue block represents the calibration sensor, and the gray block represents the origin. **(c)** A group of sliders to compare the instantaneous response for the six component of each sensor. **(d)** A row of plots that show the error between the two sensors for each force component. **(e)** A row of plots that show the estimated force for each component for the both sensors.

calibration matrix $[C] = [S]^{\dagger} = \left([S]^{\mathrm{T}}[S]\right)^{-1}[S]^{\mathrm{T}}$. The calibration matrix allows us to estimate the applied forces using the measured frequency shift signals. This estimation gives the entire force wrench. The estimation comes from:

$$\left\{\hat{F}_j\right\} = [C]\{\Delta f_i\} \quad \text{with, } i \in \{1,..,12\} \text{ and } j \in \{1,...,6\}$$

We have designed the prototype in a way that we could exploit twelve frequencies. The sensor prototype has also been designed such as to present the same forces range as the *ATI*

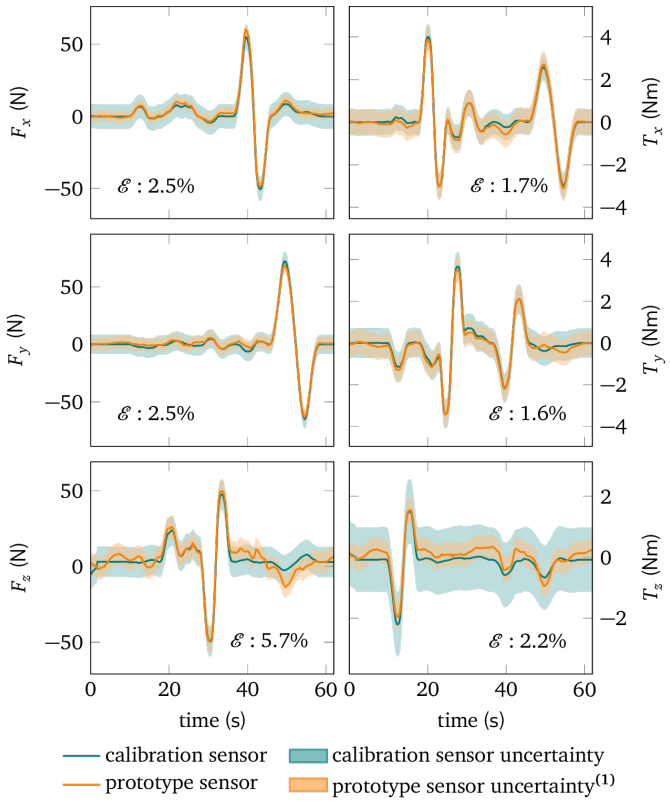

(1) uncertainty calculated from frequency shift signal noise.

Figure 19: Force estimations and comparisons between sensors. The estimation error $\mathcal{E}$ is indicated for each axis. This error is the maximum difference between the two signals along the test.

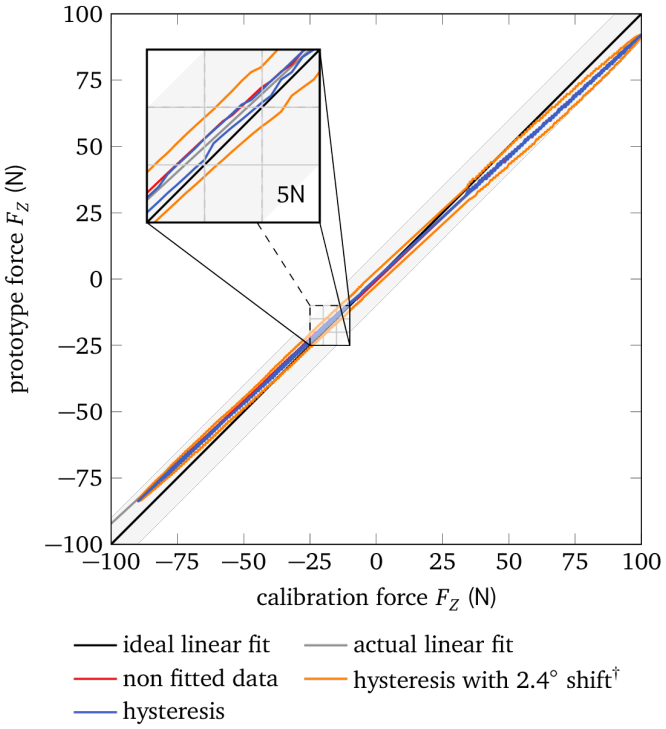

Figure 20: Comparison one-to-one between the calibration sensor and the prototype. The figure shows the force estimation of both sensors. We only present the case of the force in z-direction, because it is the worst case (see Figure 3). †The test was made in quasi-static condition.

Delta. For calibration, the applied forces range is ±100 N, which is roughly ±10 kgf. In the case of torque, the range is ±10 Nm, which represents ±10 kgf with a lever of 10 cm. As the commercial sensor, the prototype design takes into account also a security factor above the maximum forces. This factor was set to 2.

After the identification process, the prototype calibration matrix has a condition number of 76, higher than the one of the calibration sensor (46). It is important to remember that this number sets an upper limit of the estimation error. A lower condition number could lead to a more precise sensor. As it only sets an upper bound, the performances of each sensor are lower than this limit. This parameter is important in the design phase of a sensor, but it loses importance in the experimental stage.

Based on the estimation of the calibration matrix, the force can be estimated using the force sensor prototype. Comparisons between both sensors permit to evaluate the prototype performances.

The Figure 19 shows a transient response of a serie of applied force to the test-bench. The figure presents the response of the two force sensors (calibration and prototype). Each plot presents the curves of one axis, and it also presents the prototype estimation error in a percentage of the *Full Scale Output* (FSO). In table 3, we present the estimation error in force/torque units and the calibration sensor uncertainties. The estimation error is smaller than the calibration sensor uncertainty given by the manufacturer, showing the correct functioning of the prototype sensor. In the case of F_z, the prototype presents the greatest error. Figure 20 shows the relationship between the estimation of both sensors. The figure also shows calibration sensor uncertainty. The estimation of the prototype remains within this uncertainty range.

Figure 20 shows in an XY-form the same information about F_z already presented in the Figure 19. The rest of forces (F_x, F_y, T_x, T_y, T_z) are closer to the reference signal. Both axes represent forces, x-axis represents the calibration sensor and y-axis represents the prototype sensor. The ideal situation should follow a straight line with a slope of 1, but the actual fit has a slope of 0.92. This represents an error on the sensitivity of about 8%. Considering the calibration sensor as perfect, the error linearity of the prototype for F_z is 0.45% FSO (this represent the greater difference between the sensor curve (without hysteresis) and the linear estimation, all over the force range). The hysteresis is 1.3% FSO. The prototype signal has an elliptical shape, which represents a delay (not an hysteresis) between signal like *Lissajous* curve. Without the delay correction, the error represents 3.1% FSO. The phase difference between the two signals is about 2.4° in a quasi-static regime.

Repeated tests show a similar behavior in terms of the hysteresis and linearity errors. The sensitivity error is the greatest of the three errors. This can be due to the uncertainty of the cal-

	Forces (N)			Torque (Nm)		
	F_x	F_y	F_z	T_x	T_y	T_z
Prototype's estimation error	5.0	5.0	11.4	0.34	0.32	0.44
Calibration sensor uncertainty (95%)	±8.25	±8.25	±9.9	±0.6	±0.72	±1.05

Table 3: Force estimation error of the prototype compared with the calibration sensor uncertainties (with 95% of confidence). These uncertainties are given by the manufacturer.

characteristics	sensor prototype	calibration sensor
force range (±N)	660	660
force precision (N)	0.5	0.5
torque range (±Nm)	60	60
torque precision (Nm)	0.1	0.015
lower resonance (Hz)	400	1500
noise levels (±mV)	12	1
linearity (%)	0.45	0.08
hysteresis (%)	1.3	0.7
weight (g)	1560	910
diameter (mm)	140	94.5
height (mm)	130	33.3

Table 4: Sensor prototype characteristics compared to the commercial available sensors.

ibration sensor measurement or to the calibration process. This can also be due to the calibration matrix used for the comparison, which may not capture entirely the behavior of the prototype dynamics. A new calibration matrix could reduce the sensitivity error. The overall error seems acceptable for cobotic applications as stated in [38] because cobotic applications are mainly interested in the detection of the operator intention to move the robot rather than the very precise amount of applied force.

The sensor prototype performances are summarized in table 4. They are closed to those of the calibration sensor.

The precision of our sensor is thus roughly the same as that of the commercial sensor ATI which is used as a reference. This precision can even be improved by working on the reduction of electronic noise (low signal-to-noise ratio). The linearity and the hysteresis of the prototype are calculated based on the consideration of a perfect calibration sensor. In the case of linearity, the calibration sensor has a very low linearity error, so, it is fair enough to consider it as perfect. But in case of the hysteresis, the sensor hysteresis error is about the same order. Even though, their hysteresis is lower than other commercial sensors [3]. A reduction of the sensor size should be pursued to reduce the sensor mass and dimensions. As shown in Figure 19, the force estimations given by our prototype are within the uncertainty range of the calibration sensor. Consequently, we can say that our prototype is at least as good as the commercial sensor in the calibrated force range.

6. Conclusion

This article proposes a complete mechatronic design methodology dedicated to a multi-axis resonant force sensor. This device is designed to be able to estimate all 6 components of force wrench used in robotic co-manipulation applications. This sensor is based on a new technology in the context of multi-axis force measurement and its performance is very similar to that of commercially available force sensors. The literature review reveals no relevant work in the field of multi-axis resonant sensors, although this area of research holds great promise in terms of performance and safety, two key elements for collaborative robotics. A design methodology entirely dedicated to multi-axis resonant force measurement is proposed. It can be used as a basis for all future developments in this area.

A prototype sensor is designed using this methodology. It is divided into two main parts: the mechanical structure on the one hand and the monitoring and control unit on the other. The design of the mechanical structure is done in two steps: the first one focuses on the sensor's sensitive elements, based on clamped vibrating plates. The second step cleverly combines several of these sensitive modular elements to design a complete six-axis resonant force transducer. An effective control technique is proposed for the simultaneous and real-time tracking of multiple resonant frequencies. The electronic implementation of the controller, although relatively simple, is extremely efficient and robust. The calibration and validation part of the sensor prototype proves the efficiency of the entire device and confirms the effectiveness of the design approach for this type of multi-axis resonant force transducer.

Several perspectives can be proposed to improve this multi-axis resonant force sensing technology. First, the output of the resonant sensor encodes the force information in the signal frequency spectrum. In addition, the amplitude of these signals could also be used to monitor the health status of this sensor or for diagnostic purposes. This could be done in the short term. In the long term, this could help us to study the effects of the sensor's ageing process on the degradation of its performance over time. This monitoring of the sensor's health status can also be used to assess the risks of co-manipulation with humans. The sensor prototype proposed in this paper has the ability to measure all force and torque components, however new designs for other applications may require fewer axes. For example, some applications dedicated to robotic joints only require the measurement of a torque (or possibly a force measurement in the axis of this joint) and not the measurement of the entire force wrench. In this case, the design methodology proposed here can be easily adapted to the solution design dedicated to each specific application.

References

[1] Aghili F, Buehler M and Hollerbach J (2001) Design of a Hollow Hexaform Torque Sensor for Robot Joints. *The International Journal of Robotics Research* 20(12): 967–976.

[2] Alcheikh N., Mbarek S.B., Ouakad H.M., Younis M.I., (2021) A highly sensitive and wide-range resonant magnetic micro-sensor based on a buckled micro-beam. *Sensors and Actuators A: Physical* 328.

[3] ATI Industrial Automation (2016) *Capacitive 6-Axis Force Sensor: Installation and Operation Manual*.

[4] Barthod C and Gehin C (2000) New force sensor based on a double ended tuning fork. In: *Frequency Control Symposium and Exhibition, 2000. Proceedings of the 2000 IEEE/EIA International*. pp. 74 –78.

[5] Barthod C, Teisseyre Y, Géhin C and Gautier G (2003) Resonant force sensor using a PLL electronic. *Sensors and Actuators A: Physical* 104(2): 143–150.

[6] Benes E, Gröschl M, Burger W and Schmid M (1995) Sensors based on piezoelectric resonators. *Sensors and Actuators A: Physical* 48(1): 1–21.

[7] Bicchi A (1992) A criterion for optimal design of multi-axis force sensors. *Robotics and Autonomous Systems* 10(4): 269–286.

[8] Blom F (1989) *Resonant silicon beam force sensor*. Ph.D. Thesis, Twente University of Enschede, Netherlands.

[9] Bruggi M and Duysinx P (2012) Topology optimization for minimum weight with compliance and stress constraints. *Structural and Multidisciplinary Optimization* 46(3): 369–384.

[10] Cailliez J, Boudaoud M, Mohand-Ousaid A, Weill-Duflos A, Haliyo S. and Regnier S. (2019) Modeling and experimental characterization of an active MEMS based force sensor. *Journal of Micro-Bio Robotics* 15: 53–64.

[11] Castano-Cano D, Grossard M and Hubert A (2014) Multi-axis force sensing with pre-stressed resonant composite plates: An alternative to strain gauge force sensors. In: *Advanced Intelligent Mechatronics (AIM), 2014 IEEE/ASME International Conference on*. pp. 1361–1367.

[12] Castano-Cano D, Grossard M and Hubert A (2015) Development and characterization of a dynamic smart structure providing multi-axis force sensing for robotic applications. In: *Robotics and Automation (ICRA), 2015 IEEE International Conference on*. ISBN 978-1-4799-6923-4, pp. 3876–3882.

[13] Castano-Cano D, Grossard M and Hubert A (2015) Modal Decoupling for MIMO Self-Oscillating Systems - Application to Resonant Force Sensor Control. In: *Intelligent Robots and Systems (IROS), 2015 IEEE/RSJ International Conference on*. pp. 2330–2335.

[14] Castano-Cano D, Grossard M and Hubert A (2015) Multi-axis force sensing using a resonant composite piezoelectric plate: model and experiments. *Smart Materials and Structures* 24(5): 0964–1726.

[15] Chao LP and Chen KT (1997) Shape optimal design and force sensitivity evaluation of six-axis force sensors. *Sensors and Actuators A: Physical* 63(2): 105–112.

[16] Chapuis D, Gassert R, Sache L, Burdet E and Bleuler H (2004) Design of a simple MRI/fMRI compatible force/torque sensor. In: *Intelligent Robots and Systems (IROS), 2004 IEEE/RSJ International Conference on*, volume 3. pp. 2593–2599.

[17] Cheshmehdoost A and Jones B (1996) Design and performance characteristics of an integrated high-capacity DETF-based force sensor. *Sensors and Actuators A: Physical* 52(1-3): 99–102.

[18] Chuang S (1983) Force Sensor Using Double-Ended Tuning Fork Quartz Crystals. In: *37th Annual Symposium on Frequency Control. 1983*. pp. 248 –254.

[19] Dabsch A, Rosenberg C, Klug P, Stifter M and Keplinger F (2018) Multiaxial resonant MEMS force sensor. *Journal of Micromechanics and Microengineering* 28.

[20] da Rocha J, da Rocha P and Lanceros-Mendez S (2009) Capacitive Sensor for Three-Axis Force Measurements and Its Readout Electronics. *Instrumentation and Measurement, IEEE Transactions on* 58(8): 2830–2836.

[21] Desmaële D (2011) *Design of a planar resonant force sensor with an application to cell mechanics*. Ph.D. Thesis, Université Pierre et Marie Curie, 4 place Jussieu, 75005 Paris.

[22] Desmaële D, Boukallel M and Regnier S (2011) A Planar Resonant Structure Sensitive to Out-of-plane Forces. *Procedia Engineering* 25: 579–582.

[23] Ding Y., Ren Z., Wang S., Jing W., Jiang Z., Wei X. (2021) A high-resolution resonant torque sensor based on MEMS quartz resonator. *Sensors and Actuators A: Physical* 320.

[24] Dulmet B, Bourquin R and Shibanova N (1995) Frequency-output force sensor using a multimode doubly rotated quartz resonator. *Sensors and Actuators A: Physical* 48(2): 109–116.

[25] Dumora J, Geffard F, Bidard C, Brouillet T and Fraisse P (2012) Experimental study on haptic communication of a human in a shared human-robot collaborative task. In: *2012 IEEE/RSJ International Conference on Intelligent Robots and Systems (IROS)*. pp. 5137–5144.

[26] EerNisse EP and Paros JM (1983) Practical Considerations for Miniature Quartz Resonator Force Transducers. In: *37th Annual Frequency Control Symposium*. Philadelphia, USA, pp. 255–260.

[27] Fabula T, Wagner H, Schmidt B and Büttgenbach S (1994) Triple-beam resonant silicon force sensor based on piezoelectric thin films. *Sensors and Actuators A: Physical* 42(1-3): 375–380.

[28] Fukuzawa K, Ando T, Shibamoto M, Mitsuya Y and Zhang H (2006) Monolithically fabricated double-ended tuning-fork-based force sensor. *Journal of Applied Physics* 99(9): 094901 –094901–5.

[29] Gehin C, Barthod C and Teisseyre Y (2000) Design and characterisation of a new force resonant sensor. *Sensors and Actuators A: Physical* 84(1-2): 65–69.

[30] Guggenheim J. W., Jentoft L. P., Tenzer Y. and Howe R. D. (2017) Robust and Inexpensive Six-Axis Force-Torque Sensors Using MEMS Barometers. *IEEE/ASME Transactions on Mechatronics* 22(2): 838–844.

[31] Harada K, Ikeda K, Ueda T, Kohsaka F and Isozaki K (1984) Precision transducers using mechanical resonators. Technical report, Yokogawa Technical Report.

[32] Isaacson E and Keller HB (1994) *Analysis of numerical methods*. Dover Publications.

[33] Jacq C, Lüthi B, Maeder T, Lambercy O, Gassert R and Ryser P (2010) Thick-film multi-dof force/torque sensor for wrist rehabilitation. *Sensors and Actuators A: Physical* 162(2): 361–366.

[34] Kang C (2005) Performance improvement of a 6-axis force-torque sensor via novel electronics and cross-shaped double-hole structure. *International Journal of Control Automation and Systems* 3(3): 469.

[35] Kumar R., Shriram S. Y. and Indupalli A. (2017) Design and Development of Low-Cost Three Degree of Freedom Force Sensor. *International Conference on Recent Trends in Electrical, Electronics and Computing Technologies (ICRTEECT)* 1-5.

[36] Maroufi M., Alemansour H., Bulut Coskun M., Reza Moheimani S.?O.(2018) An adjustable-stiffness MEMS force sensor: Design, characterization, and control. *Mechatronics* 56: 198-210.

[37] Gasulla M., Kyungrim K., Jinwook K., Xiaoning J. and Taeyang K. (2021) Static Force Measurement Using Piezoelectric Sensors. *Journal of Sensors*

[38] Lamy X, Colledani F, Geffard F, Measson Y and Morel G (2010) Human force amplification with industrial robot : Study of dynamic limitations. In: *Intelligent Robots and Systems (IROS), 2010 IEEE/RSJ International Conference on*. pp. 2487–2494.

[39] Langdon R (1985) Resonator sensors-a review. *Journal of Physics E: Scientific Instruments* 18(2): 103–115.

[40] Lemaire E, Rochus V, Golinval JC and Duysinx P (2008) Microbeam pull-in voltage topology optimization including material deposition constraint. *Computer Methods in Applied Mechanics and Engineering* 97(45-48): 4040–4050.

[41] Li C, Zhang C and Liu G (2014) A Piezoelectric Ultrasonic Clamp for Force Feedback Arm. In: *2014 Sixth International Conference on Intelligent Human-Machine Systems and Cybernetics (IHMSC)*, volume 2. pp. 38–41.

[42] Li YJ, Sun BY, Zhang J, Qian M and Jia ZY (2009) A novel parallel piezoelectric six-axis heavy force/torque sensor. *Measurement* 42(5): 730–736.

[43] Liang Q, Zhang D, Wang Y and Ge Y (2013) Design and analysis of a novel six-component f/t sensor based on cpm for passive compliant assembly. *Measurement Science Review* 13(5): 253–264.

[44] Liu SA and Tzo HL (2002) A novel six-component force sensor of good measurement isotropy and sensitivities. *Sensors and Actuators A: Physical* 100(2-3): 223–230.

[45] Lucas I, del Real RP, Michelena MD, de Manuel V, Duch M, Esteve J and Plaza JA (2010) Resonance frequency dependence on out-of-plane forces for square silicon membranes: applications to a MEMS gradiometer. *Sensors and Actuators A: Physical* 163: 75–81.

[46] Murozaki Y, Sakuma S and Arai F (2015) Protection of wide-range QCR load sensor using robust outer case for stable detection of biosignals. In: *IEEE International Conference on Robotics and Automation (ICRA)*. IEEE, pp. 3921–3926.

[47] Nakai A., Morishita Y., Matsumoto K. and Shimoyama I. (2015) 6-axis force-torque sensor chip composed of 16 piezoresistive beams. In: *IEEE International Conference on Micro Electro Mechanical Systems (MEMS)*. pp. 730-731.

[48] Ooe H., Fujii M., Tomitori M., and Arai T. (2016) Evaluation and optimization of quartz resonant-frequency retuned fork force sensors with high Q factors, and the associated electric circuits, for non-contact atomic force microscopy. In: *Review of Scientific Instruments*87(3): 1–8.

[49] Polygerinos P, Ataollahi A, Schaeffter T, Razavi R, Seneviratne L and Althoefer K (2011) MRI-Compatible Intensity-Modulated Force Sensor for Cardiac Catheterization Procedures. *Biomedical Engineering, IEEE Transactions on* 58(3): 721–726.

[50] Safour S and Bernard Y (2017) Static force transducer based on resonant piezoelectric structure: root cause investigation. *Smart Materials and Structures* 26(5).

[51] Santis AD, Siciliano B, Luca AD and Bicchi A (2008) An atlas of physical human-robot interaction. *Mechanism and Machine Theory* 43(3): 253 – 270.

[52] Seddik B and Rouchon JF (2010) Resonant flexional piezoelectric force sensor based on the analysis of electromechanical impedance for aircraft application. In: *2010 IEEE International Conference on Industrial Technology (ICIT)*. pp. 591 –596.

[53] Sinden F and Boie R (1986) A planar capacitive force sensor with six degrees of freedom. In: *Robotics and Automation (ICRA), 1986 IEEE International Conference on*, volume 3. pp. 1806–1814.

[54] Stefanescu DM (2011) *Handbook of Force Transducers*. Berlin, Heidelberg: Springer. ISBN 978-3-642-18296-9.

[55] T. Suganya and S. Robinson (2017) Design of 2d photonic crystal based force sensor using paralleloid ring resonator. *ICTACT Journal on Microelectronics* 3(3): 425-430.

[56] Tilmans HAC, Elwenspoek M and Fluitman JHJ (1992) Micro resonant force gauges. *Sensors and Actuators A: Physical* 30(1-2): 35–53.

[57] Tosi N, David O and Bruyninckx H (2014) Action Selection for Touch-based Localisation Trading Off Information Gain and Execution Time. In: *International Conference on Robotics and Automation*. pp. 2270–2275.

[58] Volf J, Novak V, Stebila J, Kvasnova P, Ryzenko V, Novak D (2021) Measurement of static forces up to 50 N using piezo ceramics PZK 850. *Measurement* 176.

[59] Wang D, Zhang Y, Yao C, Wu J, Jiao H and Liu M (2010) Toward Force-Based Signature Verification: A Pen-Type Sensor and Preliminary Validation. *IEEE Transactions on Instrumentation and Measurement* 59(4): 752–762.

[60] Xiong L., Guo Y., Jiang G., Zhou X., Jiang L. and Liu H. (2021) Six-Dimensional Force/Torque Sensor Based on Fiber Bragg Gratings With Low Coupling. *IEEE Transactions on Industrial Electronics* 68(5):4079-4089.

[61] Yao J, Zhang H, Zhu J, Xu Y and Zhao Y (2015) Isotropy analysis of redundant parallel six-axis force sensor. *Mechanism and Machine Theory* 91: 135–150.

[62] Yong J and Rouchon JF (2011) Resonant piezoelectric force sensor using two bending differential modes. In: *2011 IEEE International Symposium on Industrial Electronics (ISIE)*. pp. 1307–1312.

[63] Zhao Y, Zhao T, Wen R and Wang H (2007) Performance Analysis and Optimization of Sizable 6-axis Force Sensor Based on Stewart Platform. In: *International Conference on Mechatronics and Automation, 2007. ICMA 2007*. pp. 2189–2193.

[64] Zhao Z., Wang D.F., Lou X., Ono T., Itoh T. (2021) An adjustable prestress based sensitivity enhancement scheme for cantilever-based resonant sensors. *Mechanical Systems and Signal Processing* 146.

Davinson Castaño Cano received the BSc degree in Engineering Physics from EAFIT University, Medellin, Colombia; obtained a MSc degree in Mechatronic Systems from Université de Tecnologie de Compiègne, France in 2012, and received his Ph.D in Engineering Science from Université de Besançon, France in 2016. He joined EAFIT University as an assistant professor in 2017, where he is a member of the Production and Logistics Management Research Group. His research interests are in the field of mobile robotics and includes visual navigation, sensor fusion and SLAM with a focus on autonomous vehicles for logistics.

Mathieu Grossard received both the Engineering diploma and the M.Sc. degree in robotics and automation from the Ecole Centrale de Nantes (France, 2005) and the Ph.D. degree in automatic control (best French PhD award from the “GDR MACS”) at Femto-St (France, 2008). He obtained the H.D.R. (Habil. for Research Supervision) degree from UPMC Sorbonne University (France, 2019). Since 2008, he has been a senior researcher at the Interactive Robotics Unit of the CEA LIST in France, where he is responsible for robotic manipulation activities. His current research interests include optimal mechanical design, modelling and advanced control of robot manipulators, compliant structures, and active-based materials actuators/sensors.

Arnaud Hubert obtained a degree in mechanical engineering in 1996, a DEA (M.Sc) degree (1997) and a Ph.D. degree (2000) in system control at the University of Technology of Compiègne, France. After a year at the Technical University of Braunschweig, Germany, in 2001, he was an associate professor at the University of Franche-Comté, France and researcher at the FEMTO-ST Institute (2002-2014). Since 2014, he is a professor at the University of Technology of Compiègne, France in the Roberval Laboratory. His research focuses on the design, modeling and control of mechatronic devices and electromechanical energy transducers. He is mainly involved in the design of innovative actuators using smart materials and in the modeling and optimization of multi-physics systems.

Credit author statement

1. **Davinson CASTANO-CANO**
    - Methodology
    - Software
    - Investigation
    - Writing - Original Draft
    - Writing - Review & Editing
2. **Mathieu GROSSARD** (corresponding author)
    - Resources
    - Validation
    - Writing - Original Draft
    - Writing - Review & Editing
    - Supervision
3. **Arnaud HUBERT** :
    - Resources
    - Validation
    - Writing - Original Draft
    - Writing - Review & Editing
    - Supervision

Davinson Castano-Cano

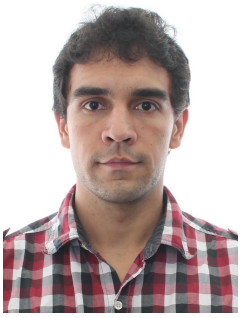

Mathieu Grossard

Arnaud Hubert

Declaration of interests

☒ The authors declare that they have no known competing financial interests or personal relationships that could have appeared to influence the work reported in this paper.

☐The authors declare the following financial interests/personal relationships which may be considered as potential competing interests: